Available online at www.sciencedirect.com
SCIENCE DIRECT®
Journal of Power Sources 136 (2004) 160–170
JOURNAL OF POWER SOURCES
www.elsevier.com/locate/jpowsour

Power-ion battery: bridging the gap between Li-ion and supercapacitor chemistries

A. Du Pasquier*, I. Plitz, J. Gural, F. Badway, G.G. Amatucci

Energy Storage Research Group Rutgers, Department of Ceramic and Materials Engineering, The State University of New Jersey, 607 Taylor Road, Piscataway, NJ 08854, USA

Received 6 April 2004; accepted 10 May 2004

Available online 28 July 2004

Abstract

A 40 Wh/kg Li-ion battery using a $Li_4Ti_5O_{12}$ nanostructured anode and a composite activated carbon $LiCoO_2$ cathode was built using plastic Li-ion processing based on PVDF-HFP binder and soft laminate packaging. The specific power of the device is similar to that of an electrochemical double-layer supercapacitor (4000 W/kg). The high power is enabled by a combination of a nanostructured negative electrode, an acetonitrile based electrolyte and an activated carbon/$LiCoO_2$ composite positive electrode. This enables very fast charging (full recharge in 3 min). The effect of electrode formulation and matching ratio on energy, power and cycle-life are described. Optimization of these parameters led to a cycle-life of 20% capacity loss after 9000 cycles at full depth of discharge (DOD).

Keywords: Activated carbon; Li-ion battery; Supercapacitor; Power-ion battery; $LiCoO_2$

1. Introduction

It is currently being debated which energy storage technology would best serve the future automotive technology where both high specific energy and power capabilities must be established [1]. The transition to 42 V systems, integrated starter-alternators, hybrid electric vehicles and purely electric vehicles, will make automobiles much more dependent on rechargeable electrochemical systems. To satisfy this demand, one approach is to improve existing technologies; the other is to invent new ones. At one end of the spectrum, Li-ion batteries [2] benefit from the highest energy densities (150–200 Wh/kg), and can now be engineered to also deliver high power (45 Wh/kg at 1000 W/kg). However, they suffer limited cycle-life (usually 500–1000 cycles at 100% DOD) and lack the ability to safely accept fast charging without Li metal deposition. On the other hand, carbon-carbon double layer capacitors [3] have virtually unlimited cycle-life, very high specific power (5000 W/kg or more), but modest energy densities (3–6 Wh/kg).

To combine the advantages of both systems, Amatucci et al. [4] invented a new class of nonaqueous hybrid devices [5] one iteration of which utilizes a nanostructured $Li_4Ti_5O_{12}$ Li-intercalation anode [6] and an acetonitrile-$LiBF_4$ electrolyte, combined with an activated carbon double-layer cathode. The combined effect of a higher output voltage and an anode of greater specific capacity results in higher energy densities than carbon/carbon supercapacitors, while maintaining a high power density and robustness [7]. Those devices typically packaged have between 10 and 13 Wh/kg, with a theoretical maximum energy density around 20 Wh/kg [8]. Specific power is approximately 1500 W/kg, and the cycle-life is excellent, with over 250,000 cycles demonstrated.

The limitation in improvement of the asymmetric hybrid energy density is mainly due to the activated carbon cathode. The specific capacity of activated carbon is proportional to the electrolyte accessible mesoporous BET specific surface area, with a maximum around 2500 m^2/g, corresponding to 120–130 F/g [9]. In order to further enhance the energy density of this system, several modifications of the cathode have been proposed. One is to replace the activated carbon with an electronically conducting polymer of higher specific capacitance and higher voltage than activated carbon. For instance, poly(fluorophenyl)thiophene of 270 F/g can be used [10]. However, the two drawbacks of electronically conducting polymers are the cycle-life, which is lower than activated carbons, and the cost of production, which in some instances may be prohibitive in industrial ap-

* Corresponding author. Tel.: +1 732 445 1653; fax: +1 732 445 1660.
E-mail address: adupasqu@rci.rutgers (A.D. Pasquier).

0378-7753/$ – see front matter © 2004 Elsevier B.V. All rights reserved.
doi:10.1016/j.jpowsour.2004.05.023

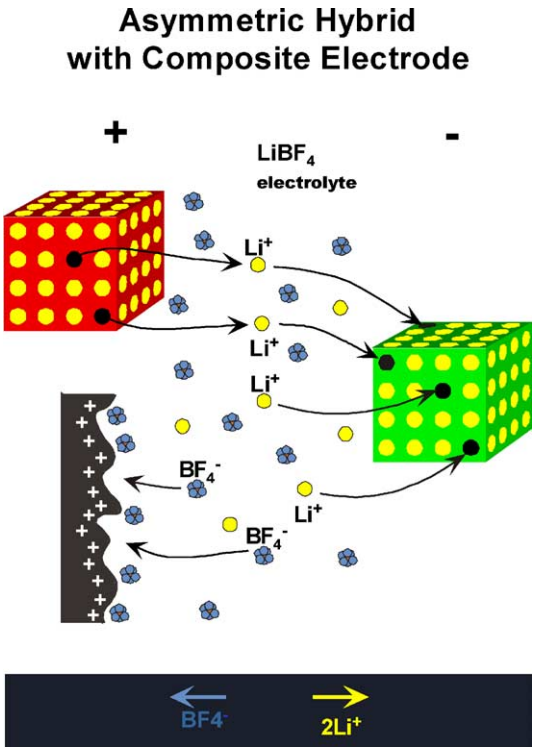

Fig. 1. Working principle of a LTO/LCO battery with added activated carbon in the cathode.

plications. On the other hand, one can fabricate composite positive electrodes consisting of a mixture of activated carbon with Li-intercalation metal oxides such as $LiMn_2O_4$ or $LiCoO_2$, and find optimal compositions that combine high energy and high power capability [11]. The content of metal oxide increases energy density by raising the average voltage and specific capacity of the cathode, while the content of activated carbon increases power capability by improving electronic conductivity and electrolyte adsorption in the cathode. In addition, the activated carbon also contributes to charge storage (Fig. 1). Of particular interest are activated carbons that possess a very high specific conductivity, due for instance, to a highly interconnected structure.

2. Experimental

2.1. Cell fabrication

Three cathode formulations of $LiCoO_2$ were prepared with either activated carbon (E350, ERACHEM Europe) termed AC hereafter, or non activated conducting carbon black (SuperP, ERACHEM Europe) termed SP hereafter. The binder used was AtoFina Kynarflex^{TM} 2801, which completed the weight fraction of powders to 100%. The electrodes were doctor-blade cast from acetone solutions plasticized with propylene carbonate. The anodes were prepared in the same way, using nano-sized $Li_4Ti_5O_{12}$ (Altair) as active material, and non-activated conducting carbon black. The electrodes formulations are summarized in Table 1.

The anode thickness was kept constant, limiting the capacity of the cells to ca 8 mAh, while the cathode thickness was varied in order to build a series of cells of matching ratios ranging from 1.2 to 2.0. Identical cells were tested for the same formulation and matching ratio. The cells were built by laminating electrodes onto aluminum current collectors etched in NaOH 10% aqueous solution and sprayed with conductive coating (Acheson colloids) in order to improve adhesion and reduce impedance. The 2″ × 1.5″ electrode-collector laminates were then assembled as batteries by hot lamination to a microporous polyolefin separator (Celgard, 25μm thick). This resulted in a bonded battery laminate of anode–cathode–anode bicell design, from which the plasticizer was extracted by immersion for 30 min in ether. The cells were then dried overnight at 85 °C (unless otherwise mentioned) under vacuum, packaged with PE/Al/surlyn laminate material (Dai Nippon), and activated in Helium filled glove-box with acetonitrile, $LiBF_4$ 2 M electrolyte.

2.2. Electrochemical testing

Electrochemical characterization was initiated with initial impedance measurements using a Solartron SI1286 impedance analyzer from 1000 to 0.1 Hz with 1 mV amplitude of perturbation signal. The cells were then subjected to a Ragone test by charging them at constant current of 0.2 A (approximately 25 C) and discharging at increasing currents from 0.2 to 2 A (25–250 C), within the voltage limits of 3.2–1.6 V. Impedance was measured again after the first Ragone test, after which the cells were reevaluated for a second Ragone test followed by constant current cycling with 0.2 A for charge and discharge and same voltage limits as the Ragone test. A Maccor series 4000 battery testing unit was used to perform these tests. After cycling, the impedance was measured again to relate any changes in capacity or power capability to impedance changes. In the latter half of the study a second characterization routine

Table 1
Formulations of the electrodes tested during this study

Electrode	Active material	Conductor	Binder
LCO 55%	$LiCoO_2$ 55%	SP or AC 20%	KynarFlex^{TM} 2801 25%
LCO 65%	$LiCoO_2$ 65%	SP or AC 10%	KynarFlex^{TM} 2801 25%
LCO 75%	$LiCoO_2$ 75%	SP or AC 5%	KynarFlex^{TM} 2801 20%
LTO 70%	$Li_4Ti_5O_{12}$ 70%	SP 10%	KynarFlex^{TM} 2801 20%

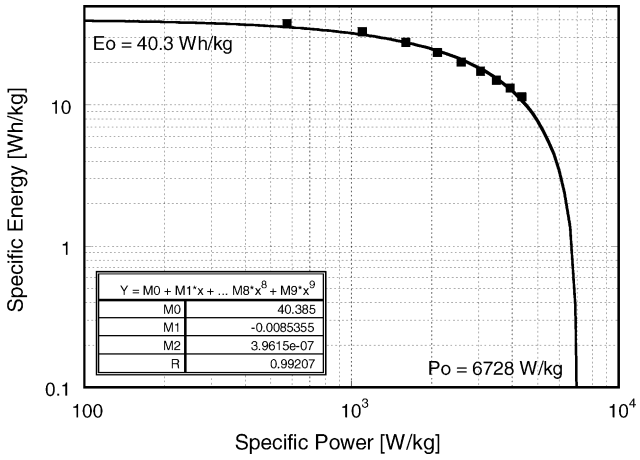

Fig. 2. Ragone plot of a 65% $LiCoO_2$–10% activated SuperP cell of matching ratio 1.2 fitted with a second-degree polynom.

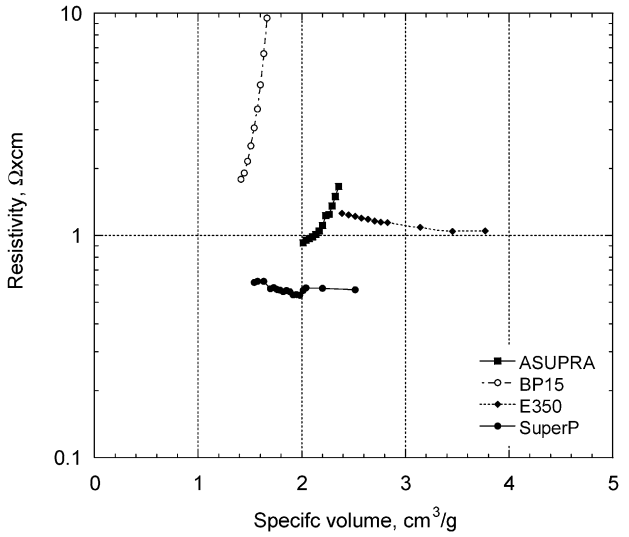

Fig. 3. Electrical resistivity vs. specific volume of various carbon materials candidates for mixing with $LiCoO_2$.

was implemented utilizing a pulse protocol consisting of approximately 10 s 4 C pulses.

For each electrode formulation and matching ratio, the Ragone plot data of each new cell was processed in the following manner: a second degree polynomial was used to fit the data which was plot in both E versus P and P versus E. The fitting was always excellent, and allowed to define the extrapolated value E_o (Wh/kg), energy when $P = 0$, and P_o (W/kg), power when $E = 0$ (Fig. 2). Since the cells were small, the weight of packaging material was close to 50% of the total cell weight. Thus, it was not included in the cell weight.

3. Results and discussion

3.1. Conductivity of activated carbons in relation with their morphology

Activated carbons can be found in a wide variety of precursor materials, BET specific surface areas and morphologies. They are usually obtained by pyrolysis of an organic precursor that can be of natural origin (wood, coconut shells, coffee beans, etc.) or synthetic origin (PVC, PAN). After pyrolysis, an activation process that raises the porosity of the carbon increases their BET specific surface area. The activation can be done by vapor steam, or oxidation by sulfuric or nitric acid. We are testing the BET specific surface area, specific capacitance and specific resistivity of three types of activated carbons. Their characteristics are listed on Table 2.

For resistivity measurements, a special piston and cylinder cell was designed. It allowed the compressing of a cylinder of carbon powder between two copper electrodes, while measuring its volume and electrical resistance. By using a constant weight of 1 g activated carbon, the density was calculated as the inverse of the cylinder volume until the maximum compression was achieved. For several piston heights h, the carbon resistivity was calculated as

$$r = \frac{R \times S}{h}, \quad \text{with } S = \text{surface of cylinder base}$$

Although this is not a true 4-electrode measurement, this method proved to be very useful for carbon comparison purposes, and the values found were close to those reported in the literature [12]. For each carbon, a curve of resistivity versus density was plotted (Fig. 3). This indicates how the resistivity changes under compression. In the case of spherical morphologies, the resistivity decreases under compression, because the interparticle contact resistance decreases. In the case of an interconnected network of particles (Super P and E350), the initial resistivity is lower, and does not decrease under compression. It rather increases, indicating that the conductive network is broken under mechanical stress. The E350 material was obtained by activation of the SuperP

Table 2
Physico-chemical characteristics of activated carbons with various morphologies

Manufacturer	Model	Morphology	Resistivity (Ω cm)	Capacitance (F/g)	BET surface area (m^2/g)
Norit	Asupra	Spherical	2	105	1483
Kuraray	BP15	Spherical	10	122	1689
Ensaco	E350	Interconnected	1	40	770
Ensaco	SuperP	Interconnected	0.5	~7	65

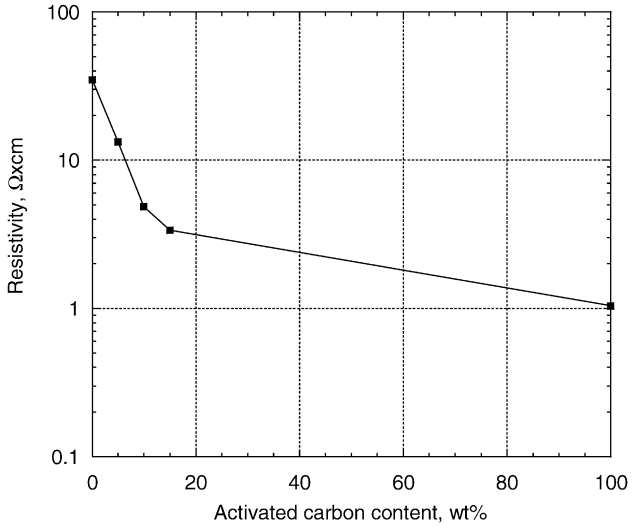

Fig. 4. Electrical resitivity of $LiCoO_2$ powder mixed with various amounts of SuperP or activated SuperP carbon.

carbon. When comparing those two carbons, the activated one has higher resistivity and higher specific volume. This is usually the consequence of the activation process. For the purpose of enhancing electrode conductivity when formed as a composite with a metal oxide, the interconnected carbons appears to be the best choice, because they will provide a lower electrode resistivity and less pressure dependancy. To answer the question whether activated or non-activated interconnected carbon results in an advantage, comparative cells were built with both.

3.2. Conductivity study of $LiCoO_2$ and activated carbon mixtures

Mixtures of $LiCoO_2$ and E350 activated carbon were prepared by high energy milling the powders for 10 min with a Spex mill using stainless-steel media. The conductivity cell described above was used for measuring conductivity and density of the powders at the maximum compression achievable. The addition of up to 15 wt.% of activated carbon resulted in a sharp decrease in resistivity of one order of magnitude, while adding more carbon has less effect, bringing the resistivity closer to the 1 Ω cm of pure activated carbon (Fig. 4). No noticeable change in specific volume of the powder mixes occurred while adding up to 15 wt.% of activated carbon.

3.3. Mixture capacity and matching ratio considerations

Activated carbon contributes to the capacity of the cathode by adsorption of BF_4^- anions on its double-layer. Specific capacity was measured to be 25 mAh/g in $LiBF_4$ 1 M-PC electrolyte versus a lithium electrode, in the same voltage range as $LiCoO_2$ (4.2–2.6 V). Under the same conditions, the measured capacity of the $LiCoO_2$ used in this study was 135 mAh/g. Thus, we can calculate the capacity of various mixtures of active powders, by either neglecting or including the capacity of the activated carbon. The three compositions prepared for this study and their calculated capacities are summarized in Table 3.

Table 3
Specific capacity of activated carbon–$LiCoO_2$ mixtures with or without accounting for the activated carbon capacity

$LiCoO_2$ (wt.%)	AC (wt.%)	Mixture capacity (LCO + AC) (mAh/g)	Mixture capacity (AC neglected) (mAh/g)
55	20	105.7	99
65	10	120.3	117
75	5	128.1	126.6

In order to balance the capacities of negative to positive electrode it appeared that, in this range of compositions, neglecting the contribution of the AC did not lead to more than 7% error in the cathode capacity calculation. Due to its high specific capacity the component most sensitive to the matching ratio is $LiCoO_2$. Therefore, the matching ratio calculation, defined as the ratio of positive to negative active materials weight, did not include the weight of activated carbon. In the design of the cells, the standard matching ratio was targeted at equaling the capacities of $Li_4Ti_5O_{12}$ and $LiCoO_2$. Knowing their respective capacities of 160 and 135 mAh/g, the target matching ratio was 1.18. There is, in principle, no need to add extra-capacity in the positive to allow for the formation of an extended solid electrolyte interface (SEI) on the negative electrode as the voltage of $Li_4Ti_5O_{12}$ is higher than the decomposition voltage of the electrolyte. Therefore, the $Li_4Ti_5O_{12}/LiCoO_2$ system has some of the advantages of a Li-ion battery without the inconvenience of having a SEI layer.

3.4. Effect of cathode formulation on energy density

3.4.1. Effect of the matching ratio and $LiCoO_2$ content

The energy density of the cells determined by extrapolation of the Ragone plots to zero current (cf. Section 2) was plotted as function of matching ratio (Fig. 5). The first observation is that energy density increases with $LiCoO_2$ content in the cathode. This is expected as $LiCoO_2$ has a higher specific capacity and higher average voltage than activated carbon. The second observation is that the matching ratio does affect the energy density, and the highest energy densities are obtained for a matching ratio around 1.5. This is higher than the theoretic matching ratio of 1.18, and may result from the difference in capacity utilization between the nano-$Li_4Ti_5O_{12}$ and the $LiCoO_2$. The former having better utilization, delivers close to its true capacity of 160 mAh/g. In contrast, it is very likely that $LiCoO_2$ may only be delivering 110 mAh/g instead of 135 mAh/g at the minimum applied current density utilized to calculate the Ragone plot extrapolation. At a matching ratio lower than 1.5, the anode is not fully utilized, thus the energy is lower.

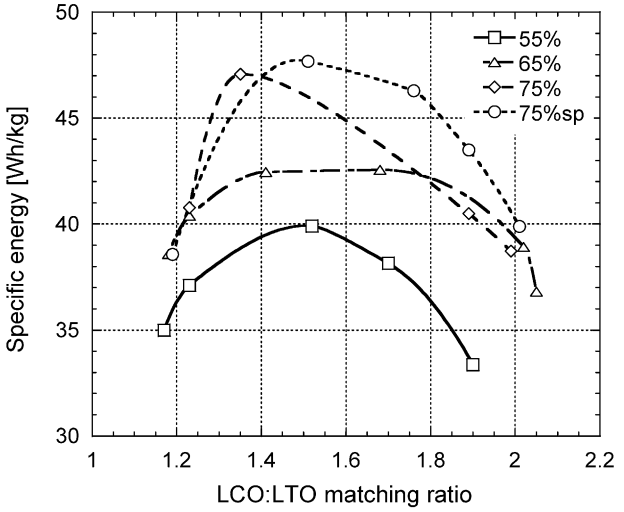

Fig. 5. Specific energy vs. matching ratio of LTO/LCO cells made with 55, 65, 75% LCO mixed with 20, 10, 5% activated SuperP, as well as 75% LCO mixed with 5% SuperP.

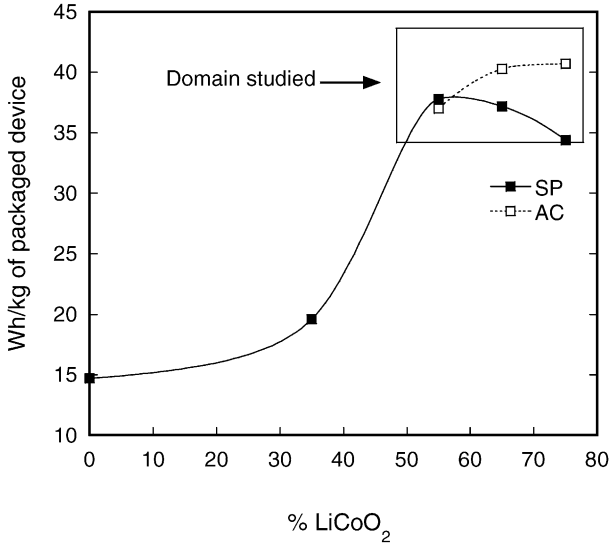

Fig. 7. Specific energy vs. LCO content mixed with SuperP or activated SuperP carbon for LTO/LCO cells of matching ratio close to 1.2.

At a matching ratio higher than 1.5, the cathode is not fully utilized, and also results in a decrease in observed energy densities.

3.4.2. Effect of the activated conducting carbon

We have also compared the effect of AC versus SP on the maximum energy of the cells, for a similar matching ratio of 1.2. See the Ragone plots for these cells on Fig. 6. At increasing LCO content, we observe a greater difference between activated and non-activated SuperP, namely, an increasing specific energy with AC, while it decreases with SP (Fig. 7). We attribute this effect to the lower electrolyte retention with SP, which become noticeable when carbon content is low. This results in lower utlization of the SP-$LiCoO_2$ electrode, while it is still fully utilized with AC. Thus, with SP, greater matching ratio than with AC is necessary to attain optimum energies. We have then plotted the highest energy obtained for each $LiCoO_2$ content regardless of matching ratio, starting from pure activated carbon (asymmetric hybrid supercapacitor) up to 75% $LiCoO_2$. This demonstrates that a specific energy ranging from 40 to 47 Wh/kg can be obtained in the range of formulations considered (Fig. 8). The next step is to narrow down to the formulations that optimize power and cycle-life.

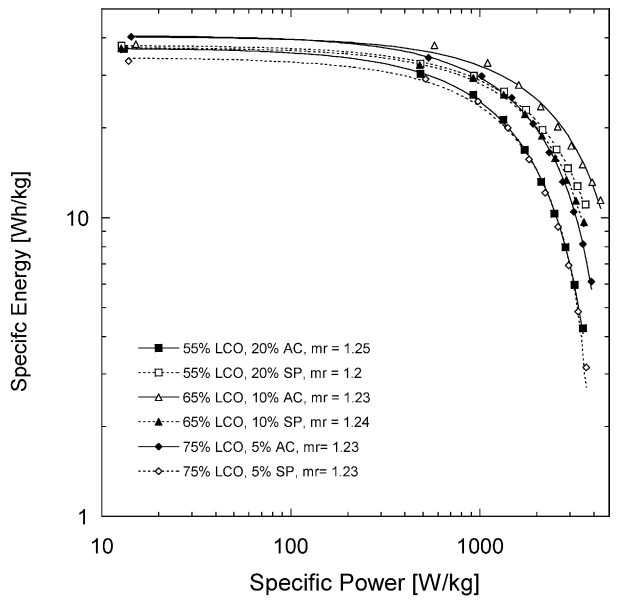

Fig. 6. Ragone plots of cells made with 55, 65, 75% LCO mixed with 20, 10, 5% activated SuperP (—) or SuperP (- - -), at matching ratio close to 1.2.

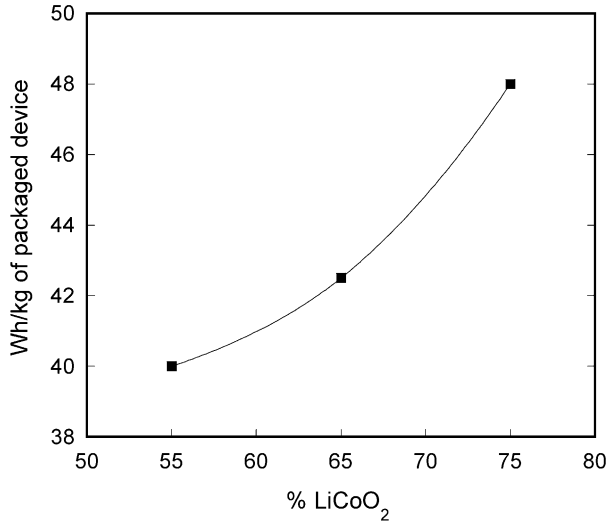

Fig. 8. Specific energy vs. LCO content in LTO/LCO cells, regardless of matching ratio.

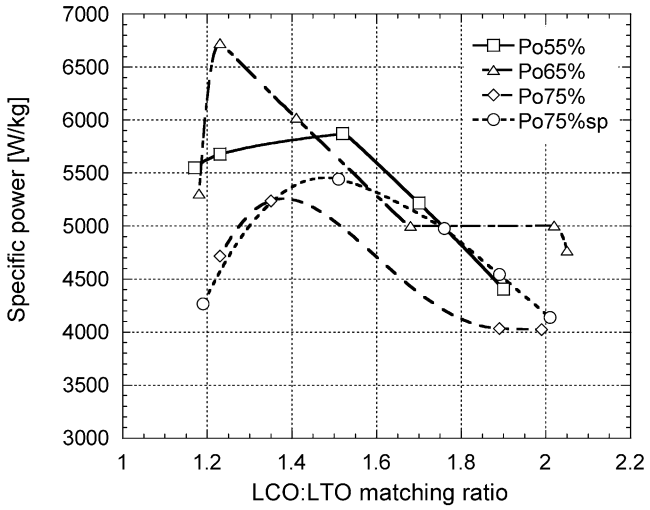

Fig. 9. Maximum specific power vs. matching ratio of LTO/LCO cells made with 55, 65, 75% LCO mixed with 20, 10, 5% activated SuperP, as well as 75% LCO mixed with 5% SuperP.

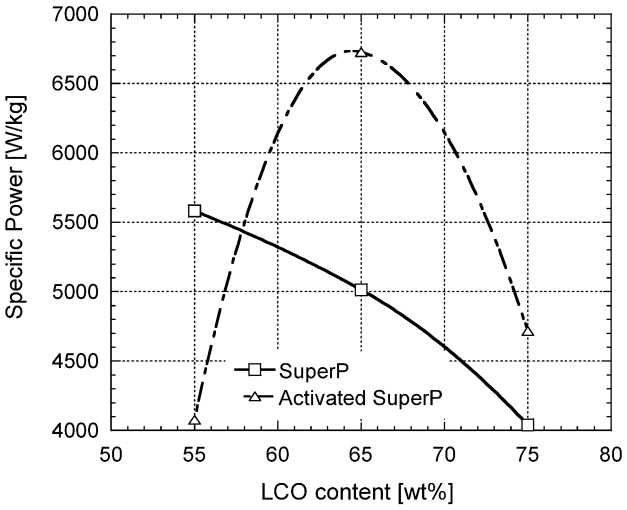

Fig. 11. Maximum specific power vs. LCO content for LTO/LCO cells made with 55, 65, 75% LCO mixed with 20, 10, 5% activated SuperP at matching ratio close to 1.2.

3.5. Effect of cathode formulation on power density

3.5.1. Effect of the matching ratio and $LiCoO_2$ content

The Ragone plots were extrapolated for maximum power of the cells, when energy reaches zero, which is analogous to a theoretical peak power. The values are plotted as a function of matching ratio, for the various $LiCoO_2$ contents (Fig. 9). The first observation is that maximum power decreases when matching the ratio increases. This is related to the fact that the cathode thickness increases with matching ratio, since the anode thickness was kept constant. Secondly, we find higher maximum powers at higher activated carbon contents. This is attributed to better electronic conductivity of these electrodes, as well as higher electrolyte content due to the adsorption on the activated carbon. However, it should be noted that the presence of activated carbon also increases electrode thickness, which handicaps diffusion in the electrode. This may explain why the 65% composition delivered higher power than the 55% composition. The observation of the derivative curves of the galvanostatic charge–discharge confirms that less polarization occurs in the 65% LCO composition, and the charging peak is shifted to ca 100 mV lower potential (Fig. 10).

3.5.2. Effect of the activated conducting carbon

We performed a comparison of AC versus SP for the three LCO contents at a similar matching ratio of 1.2. In the case of SP, the maximum power decreases when LCO content

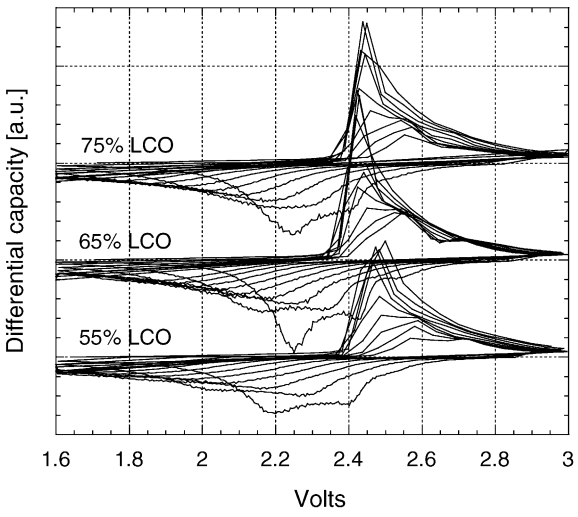

Fig. 10. Derivative of capacity vs. potential for LTO/LCO cells made with 55, 65, 75% LCO mixed with 20, 10, 5% activated SuperP at matching ratio close to 1.2.

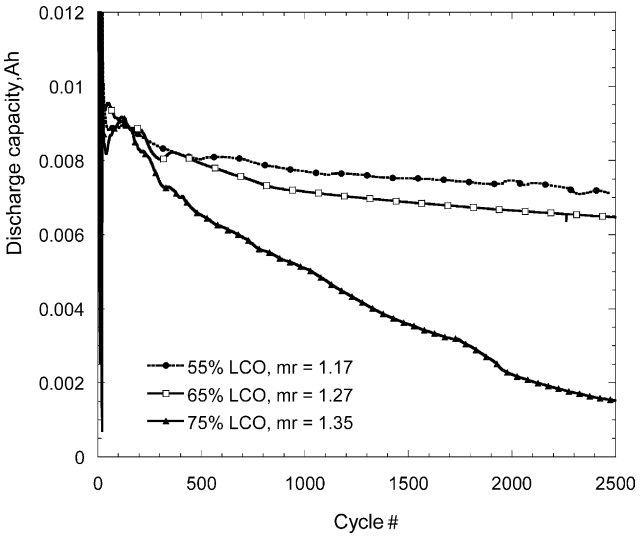

Fig. 12. Discharge capacity vs. cycle number for LTO/LCO cells made with 55, 65, 75% LCO mixed with 20, 10, 5% activated SuperP at matching ratio close to 1.2. (Galvanostatic cycling at 20C charge–discharge rate between 1.6 and 3.0 V.)

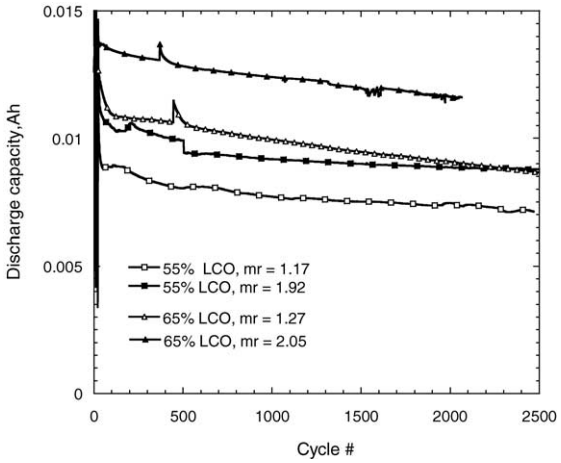

Fig. 13. Discharge capacity vs. cycle number for LTO/LCO cells made with 55 and 65% LCO mixed with 20 and 10% activated SuperP at matching ratio close to 1.2 or 2.0. (Galvanostatic cycling at 20 C charge–discharge rate between 1.6 and 3.0 V.)

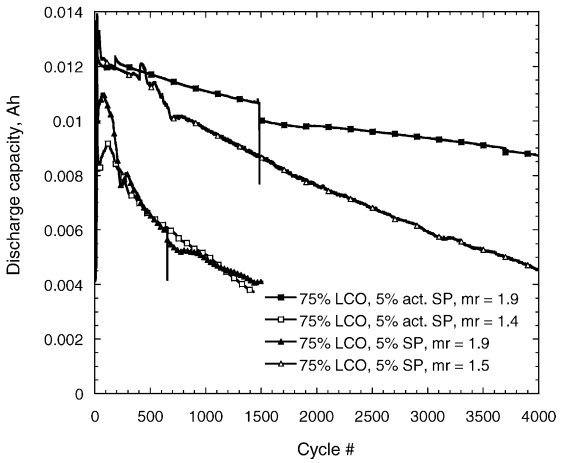

Fig. 14. Discharge capacity vs. cycle number for LTO/LCO cells made with 75% LCO and 5% SuperP or activated SuperP carbons, at matching ratio close to 1.5 or 1.9. (Galvanostatic cycling at 20 C charge–discharge rate between 1.6 and 3.0 V.)

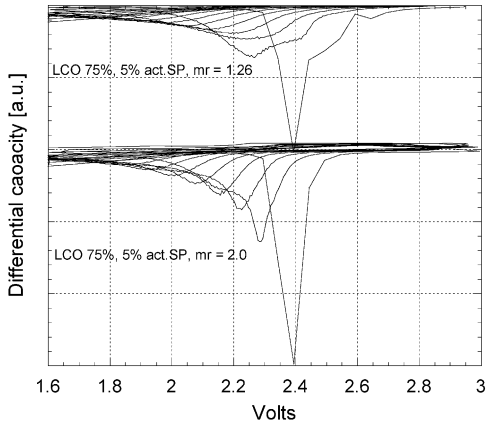

Fig. 15. Derivative of capacity vs. potential for LTO/LCO cells made with 75% LCO mixed with 5% activated SuperP at matching ratio close to 1.2 or 2.0.

increases. In the case of AC, the power goes through a maximum at 65% LCO, but is lower at 55% LCO (Fig. 11). At high carbon contents, percolation is not an issue as opposed to electrode thickness and carbon conductivity. Since SP is denser and more conductive than AC, it is understandable that the 55% LCO formulation has higher power with SP. In the 75% LCO formulation, the use of AC is not as effective as for the use of AC in the 65% LCO electrode, but still yields to higher power than the SP. This may be related to less electronic percolation as well as less electrolyte adsorbed by the activated carbon than in the 65% LCO-10% AC.

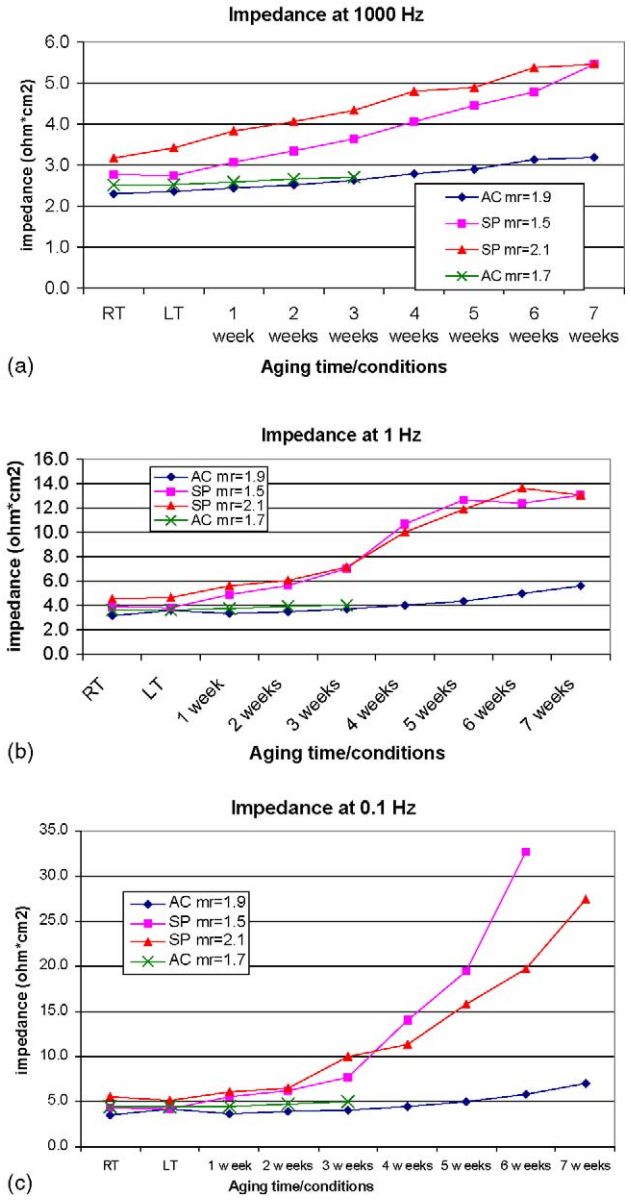

Fig. 16. Weekly impedance evolution at 1000 Hz (a), 1 Hz (b) and 0.1 Hz (c) for power-ion cells subjected to a pulse protocol cycling, showing the effect of AC vs. SP carbon, using two matching ratios for each type of carbon.

3.6. Effect of cathode formulation on cycle-life

All cells were tested at a constant charge–discharge current of 0.2 A (∼25 C) between 3.0 and 1.6 V. We found three major parameters affecting the cycle-life: the cell matching ratio, the conducting carbon content and its nature. For making meaningful conclusions for one parameter, it is necessary to fix the other.

In a first set of experiments, the effect of the activated carbon content at or around the theoretic matching ratio of 1.18 was compared. In these conditions, we observed that the cycle-life increased when the activated carbon content

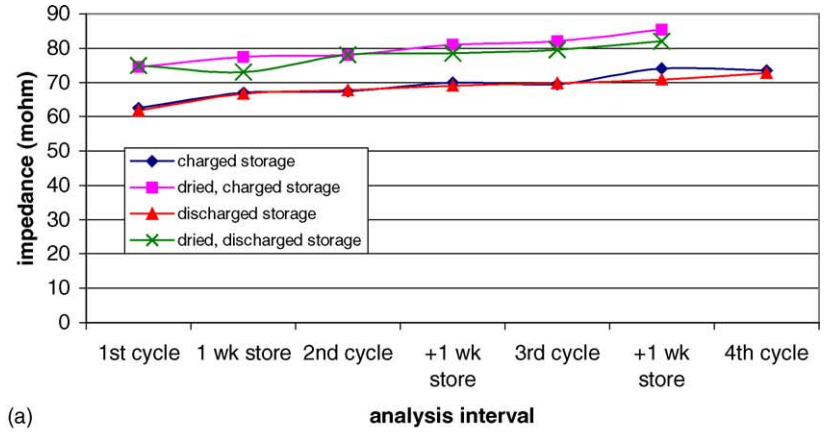

(a)

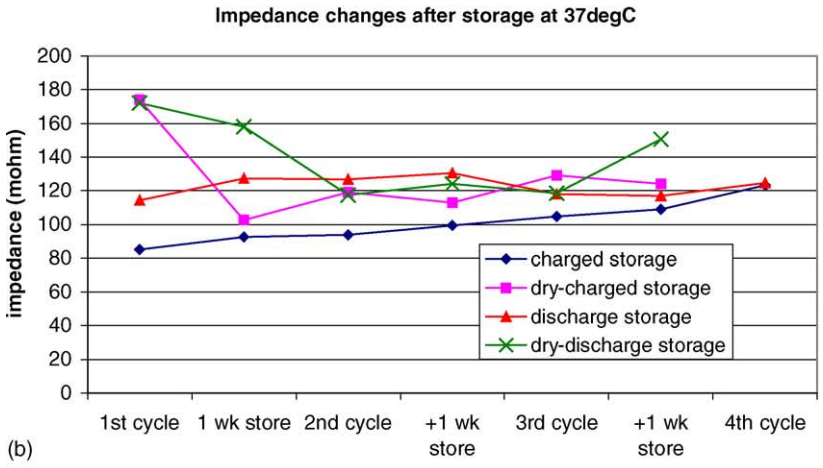

(b)

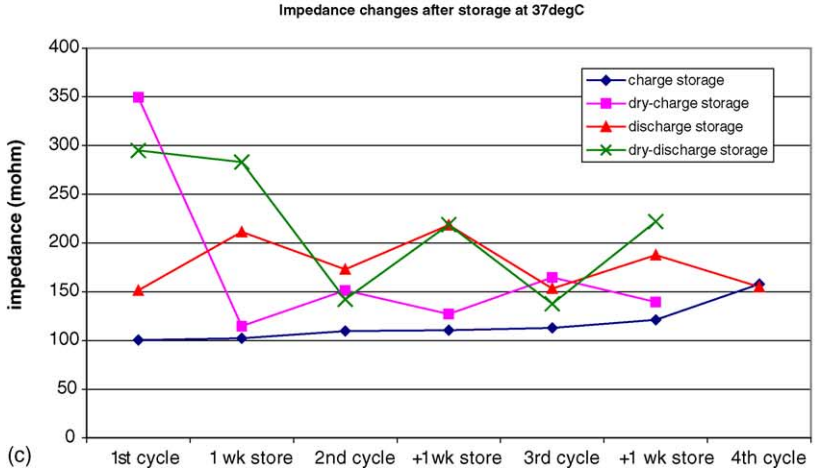

(c)

Fig. 17. Weekly impedance evolution upon storage at 1000 Hz (a), 1 Hz (b) and 0.1 Hz (c) for power-ion cells using 65% $LiCoO_2$, 10% AC, 1.7 matching ratio. The cells were either dried at 85 °C or 120 °C, and stored at 37 °C either in the charged or discharged state.

increased, even when this resulted in slightly lower matching ratios (Fig. 12).

In a second set of experiments, for a fixed electrode formulation, we did observe the effect of matching ratio. In the case of 65 and 55% LCO formulations, there is an initial capacity drop, which increases when the matching ratio is low. Afterwards, the capacity fade stabilizes, with a slope that does not seem to depend on the matching ratio, but which is higher for the 65% LCO composition (Fig. 13). For the 75% LCO formulation, we observe a higher fade, and an even greater effect of the matching ratio. Better cycle-life is obtained with a high matching ratio (1.9) and with AC instead of SP (Fig. 14).

To understand the effect of matching ratio on capacity fade, we plotted the derivative of the discharge curves for 75% LCO-5% AC cells of matching ratio 1.26 and 2.0. With matching ratio 1.26, we observe two discharge waves, indicating two phase transitions in the material, while there is only one discharge peak with a matching ratio of 2.0 (Fig. 15). This is because at low matching ratio, $LiCoO_2$ is more delithiated during charge, which can induce damage to the structure [6].

3.7. Impedance

The majority of the applications, whether automotive, electronic, or industrial involving this technology will entail the ability to deliver extended pulses. Key to the successful implementation of this technology will be the ability to maintain this pulse delivering capability, which relies exclusively on the maintenance low impedance. In light of this requirement a comparative study was undertaken examining and improvement of the impedance evolution as a function of both cycling and storage.

Three differing configurations of plastic cells were fabricated based on the most favorable results of the previous experiments, i.e. using 65% LiCoO2 and 10% carbon. Inverted bicells (that is the cathode is in the center with the two anodes on each side) were fabricated, $2'' \times 3''$ or $1.5'' \times 2''$. Unless otherwise stated, the cells were packaged, dried overnight at 85 °C under vacuum and activated with 2 M $LiBF_4$ in acetonitrile. In some cases, as noted, the cells were dried at 120 °C under vacuum and then packaged inside the glovebox. For the electrolyte study, one group of cells was activated with a standard Li-ion electrolyte of 1 M $LiPF_6$ in EC: DMC.

The first study was to evaluate the progression and origin of impedance under an intermittent, semi-strenuous (4 C) extended (approximately 10 s) pulse peak. Impedance measurements were taken at 1000, 1, 0.1 Hz after weekly intervals of cycling under the pulse protocol comparing SP versus AC and different matching ratios. Initially 4 cells were made for each category, AC mr = 1.9, SP mr = 2.1, and SP mr = 1.5. Later, four additional cells were made, AC mr = 1.7. These cells were used to monitor impedance at different frequencies at weekly intervals. Each cell spent a week at 25 °C, then at −30 °C and finally continuing at 25 °C using a pulse discharge cycling protocol. Fig. 16a–c show impedance changes at different frequencies over the test time for the four groups. In all groups, impedance gradually increases as the weeks go by, with little stabilization. Most of the impedance changes are at the lower frequencies of 1 and 0.1 implying the development of diffusional impedance. There was relatively little change in the higher frequency 1000 Hz IR region. The AC (activated carbon) samples perform significantly better than the SP (carbon black) samples. Justifying the power ion configuration using activated carbon based composites.

The second study of the series was to investigate the development of impedance and capacity loss as a function of storage time in the charged and discharged state at elevated temperature. Three groups of four cells each were made for this study. They were all based on the best configuration found in the previous study, AC mr = 1.7. One group was

Table 4
Effect of drying and state of charge on reversible and irreversible capacity loss of power-ion cells during a combination of pulse discharges and storage at 37 °C

ID	Storage state/time	Cycle capacity (mAh)	Reversible loss (%)	Irreversible loss (%)
Standard cell	Charge/1st week	100	50	3.5
	Charge/2nd week		37	2
	Charge/3rd week		39	1
Dried cell	Charge/1st week	96	25	1.5
	Charge/2nd week		17	1
	Charge/3rd week		18	<1
Standard cell	Discharge/1st week	101		0
	Discharge/2nd week			0
	Discharge/3rd week			<0
Dried cell	Discharge/1st week	101		<0
	Discharge/2nd week			<0
	Discharge/3rd week			<1

used for discharge storage, one for charge storage and the third group was dried at 120 °C under vacuum (as opposed to 85 °C), packaged in the glovebox and divided into two groups of two for charge and discharge storage. They were cycled using a combination of 0.5 C and the pulse protocol for 1 week and then stored at 37 °C in either charged or discharged state for 1 week. This pattern is looped. Table 4 shows the average reversible and irreversible capacity loss for the average of these cells.

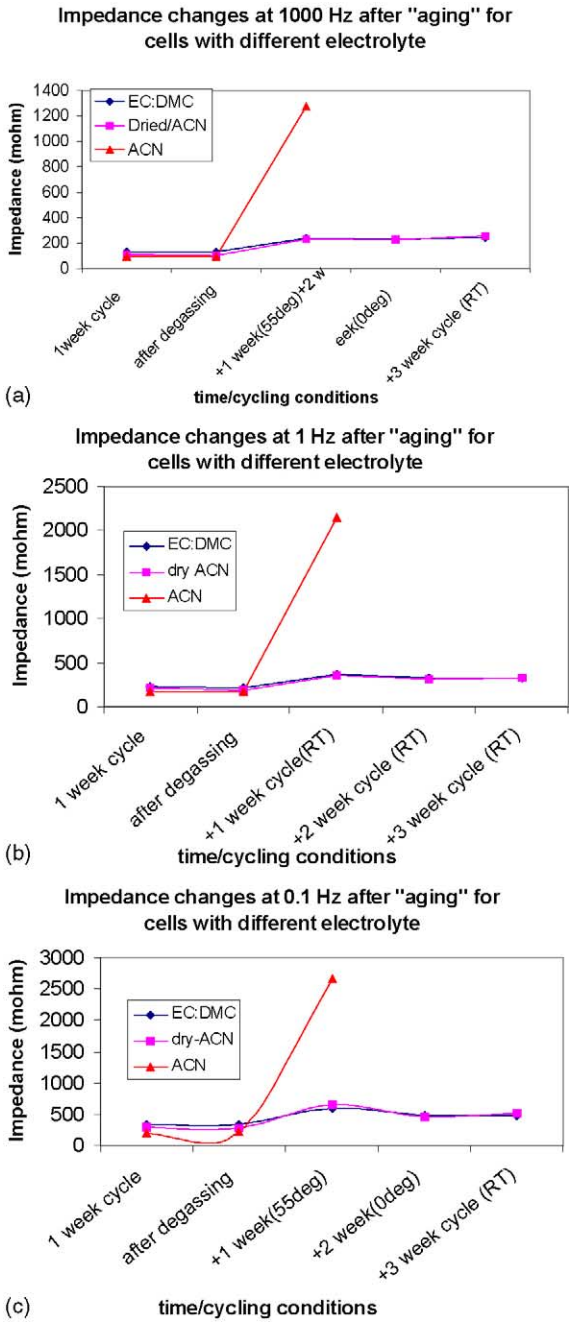

Fig. 18. Weekly impedance evolution at 1000 Hz (a), 1 Hz (b) and 0.1 Hz (c) for power-ion cells using 65% $LiCoO_2$, 10% AC, 1.6. The electrolyte was $LiBF_4$/ACN, or $LiPF_6$/EC: DMC (all dried under vacuum in antechamber at 85 °C), and four were dried at 120 °C, packaged inside the glovebox and activated with $LiBF_4$/CAN. The cells were subjected to a pulse protocol cycling at various temperatures.

Examination of the results reveals that elevated temperature irreversible capacity loss is non-existent for those cells which are stored in the discharged state. Cells which have been extensively dried at 120 °C under vacuum as opposed to 85 °C show a 50% reduction in both the reversible and irreversible capacity loss. The impedance results for the stored cells are shown in Fig. 17a–c. Overall, the initial impedance for the 120 °C dried samples is slightly higher. Charged storage impedance is slightly higher than the discharged storage impedance. Impedance for all samples seemed to be relatively stable and constant throughout all frequency ranges.

The final study was to investigate the progression of impedance and gassing utilizing a set of 12 AC cells of matching ratio of 1.6, similar to the ones previously utilized. Four were activated with standard $LiBF_4$/ACN, four with $LiPF_6$/EC: DMC (all dried under vacuum in antechamber at 85 °C (designated Standard)), and four were dried at 120 °C, packaged inside the glovebox and activated with $LiBF_4$/ACN (designated Dry). They were tested by a combination 0.5C cycling and pulse cycling for 1 week at 24 °C, then 1 week at 55 °C, then 1 week at 0 °C and then continuing at 24 °C. Impedance and gas volume were monitored weekly. Fig. 18a–c show the average impedance changes for this series of cells after each aging condition at the three measured frequencies.

One week of cycling at 55 °C resulted in enormous increase of impedance of the standard cells with the $LiBF_4$ acetonitrile electrolyte. The elevated temperature cycling resulted in an initial doubling of the impedance of the 120 °C dried $LiBF_4$ acetonitrile cells and the $LiPF_6$ EC: DMC cells which then lowered as cells were cycled at 24 °C. Cycling for a week at 0 °C had little effect on the aforementioned two sets of remaining cells.

Table 5 shows gas evolution for these cells. The values shown are the total gas accumulated in an average of four cells having the specified electrolyte and testing conditions. The 120 °C dried $LiBF_4$ acetonitrile cells displayed the lowest gas evolution. Cycling at 0 and 24 °C did not increase the overall gas evolution.

Table 5
Effect of electrolyte and drying on gas evolution in power-ion cells during cycling at various temperatures

Electrolyte/cycling temperature	Gas formed (ml)
Standard CAN/55 °C	14
Dry ACN/55 °C	5
Dry ACN/0 °C	4
Dry ACN/RT	4
EC: DMC/55 °C	17
EC: DMC/0 °C	16
EC: DMC/RT °C	15

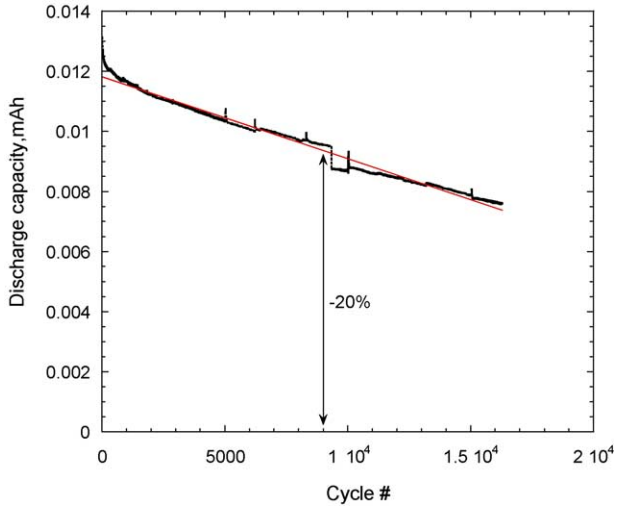

Fig. 19. Discharge capacity vs. cycle number for LTO/LCO cells made with 55% LCO and 20% activated SuperP carbon, at matching ratio of 1.67. (Galvanostatic cycling at 20C charge–discharge rate between 1.6 and 3.0 V.)

4. Discussion

As it is often the case, optimal compositions and matching ratios differ depending on which property one seeks to optimize. As far as energy is concerned, the highest LCO content of 75%, and a matching ratio around 1.4–1.5 gave the best results, with a maximum energy of 48 Wh/kg. As far as power is concerned, the highest specific powers were obtained with the 65% LCO composition, and at a lower matching ratio (1.2–1.3), e.g. a thinner cathode.

Regarding the effect of the nature of conducting carbon, activated versus non-activated the use of activated carbon is beneficial for all properties, except when the carbon content is so high in the electrodes (55% $LiCoO_2$) where little improvement is realized.

The best results for cycle life are obtained for 55% LCO contents, and high matching ratio utilizing AC. An optimized cell could achieve 9000 cycles with a capacity loss of 20% (Fig. 19). Thus, the most contradictory properties seem to be power and cycle-life, because the former requires the lowest matching ratio, while the later requires the highest matching ratio. This however assumes a constant maximum cutoff voltage of 3.0 V, and a constant anode thickness. Electrochemically, cutoff voltages and matching ratio are equivalent. Low matching ratio push the cathode to higher delithiation, hence the accelerated degradation. To optimize power and cycle-life simultaneously, one could first optimize the cathode thickness for power and energy, and then adjust the maximum cutoff voltage or anode thickness for better cycle-life. It is however not trivial to predict which approach would lead to best results, and appears to be beyond the scope of this paper.

With respect to impedance, the beneficial effect of AC is clearly shown in the significant reduction of impedance rise upon aging. We also demonstrated the importance of better drying of the electrodes, which contributed also to reduce impedance rise and gas generation. The comparison of ACN, $LiBF_4$ electrolyte with EC: DMC, $LiPF_6$ did not reveal any direct impact on impedance rise or gassing, showing it had sufficient overall stability in this system.

5. Conclusions

We have developed and partially optimized a composite electrode hybrid $Li_4Ti_5O_{12}$/($LiCoO_2$: activated carbon) cell that combines high specific power and good cycle-life [11]. Among the cells tested, the best compromise for energy, power and cycle-life appears to be at 65% $LiCoO_2$ content, 10% interconnected activated carbon and a matching ratio greater than 1.5. This type of cell is in our view, very promising for many application where fast charge, high power and extended cycle-life are required. We demonstrated full charge in 3 min (20 C), which combined with an energy density of 40 Wh/kg, is very attractive for applications such as power-tools and digital cameras. Although the cycle-life is one to two orders of magnitude lower than that of carbon/carbon supercapacitors and asymmetric C/$Li_4Ti_5O_{12}$ devices, advantages include one order of magnitude higher specific energy, reduced self-discharge and reduced gassing. Further improvement can be envisioned by the adoption of improved intercalation material/activated carbon composites.

Acknowledgements

The authors would like to thank the US government for their support of this research.

References

[1] A. Chu, P. Braatz, J. Power Sources 112 (2002) 236–246.
[2] A.M. Lackner, E. Sherman, P.O. Braatz, J.D. Margenum, J. Power Sources 104 (2002) 1–6.
[3] E. Faggioli, P. Rena, V. Danel, X. Andrieu, R. Mallant, H. Kahlen, J. Power Sources 84 (1999) 261–269.
[4] G.G. Amatucci, F. Badway, A. Du Pasquier, T. Zheng, J. Electrochem. Soc. 148 (2001) A930.
[5] US Patent 6,252,762.
[6] G.G. Amatucci, J.M. Tarascon, L.C. Klein, J. Electrochem. Soc. 143 (1996) 1114.
[7] L. Kavan, J. Procházka, T.M. Spitler, M. Kalbáč, M. Zukalová, T. Drezen, M. Grätzel, J. Electrochem. Soc. 150 (2003) A1000.
[8] A.D. Pasquier, I. Plitz, J. Gural, S. Menocal, G. Amatucci, J. Power Sources 113 (2003) 62–71.
[9] H. Shi, Electrochim. Acta 10 (1996) 1633–1639.
[10] A. Du Pasquier, A. Laforgue, P. Simon, G.G. Amatucci, J.-F. Fauvarque, J. Electrochem. Soc. 149 (2002) A302–A306.
[11] US Patent 6,517,972.
[12] J. Gamby, P.L. Taberna, P. Simon, J.F. Fauvarque, M. Chesneau, J. Power Sources 101 (2001) 109–116.